

Antiproton and proton collisions with the alkali metal atoms Li, Na, and K

Armin Lühr and Alejandro Saenz

(Dated: November 2, 2021)

Single-electron ionization and excitation cross sections as well as cross sections for excitation into the first excited p state of the alkali metal atoms Li(2s), Na(3s) and K(4s) colliding with antiprotons and protons were calculated using a time-dependent channel-coupling approach. For antiprotons an impact-energy range from 0.25 to 1000 keV and for protons from 2 to 1000 keV was considered. The target atoms are treated as effective one-electron systems using a model potential. The results are compared with theoretical and experimental data from literature and calculated cross sections for antiproton-hydrogen collisions. For proton collisions a good overall agreement is found which confirms the present numerical approach, whereas discrepancies are found between the present antiproton cross sections and those calculated by Stary et al., J. Phys. B **23**, 263 (1990).

PACS numbers: 34.50.Fa

I. INTRODUCTION

Collisions with alkali metal atoms as targets have been studied in numerous experimental and theoretical works over many years. Among these studies a number of efforts deal with proton-alkali metal atom collisions [1, 2, 3, 4, 5, 6, 7, 8, 9, 10, 11, 12, 13, 14, 15, 16] and a smaller number of attempts address collisions including antiprotons as projectiles [17, 18]. One reason for the attractivity of alkali metal atoms is that they are relatively easy to access experimentally as well as theoretically which opens up the possibility for detailed comparisons. The given shell structure of the alkali metals suggests in a theoretical description the application of a quasi-one-electron model for the outermost loosely bound electron. The electron is then described by means of a model potential formed by the Coulomb potential of the nucleus and an effective potential representing the frozen inner-shell electrons. In particular, Li and Na atoms colliding with protons and electrons have been in the focus of the investigations so far. Whereas the literature on alkali metal atoms collisions dealing with antiprotons as projectile is still sparse compared to the treatment of protons and electrons. In order to obtain cross sections for ionization of Li by antiproton impact a continuum-distorted-wave eikonal-initial-state model has been used by McCartney et al. [18]. Furthermore, an optical-potential description of collisions of antiprotons with Li and Na has been provided by Stary et al. [17]. No experimental data are available for the considered antiproton-alkali metal atom collision systems yet due to the lack of appropriate low-energy antiproton sources. This may also be the reason for the relatively small interest in antiproton-alkali metal collisions compared to their proton counterparts until now. However, the upcoming Facility for Antiproton and Ion Research (FAIR) with its incorporated Facility for Low energy Antiproton and Ion Research (FLAIR) [19] will provide the necessary experimental conditions in the near future and is therefore expected to attract further attention to the field of antiproton collisions.

The primary motivation of this work is to shed more light on the antiproton-alkali metal collision systems and to provide a consistent data base for Li(2s), Na(3s) and K(4s) atom collisions with antiprotons and protons in a large energy range. It starts at low energies $E = 0.25$ keV where the collision processes depend considerably on the projectile and ranges up to high energies $E = 1000$ keV where the antiproton and proton collision systems are supposed to show the same behavior due to the expected applicability of the first Born approximation. The calculations for collisions with proton projectiles are considered to be valuable in two aspects. On the one hand, the proton results – especially for Li targets – can be compared in detail with literature values. This way the proton results can be utilized in order to test the present method and its implementation which is the same for protons and antiprotons. Furthermore, new theoretical ionization and excitation cross sections for proton collisions – especially for K targets – are provided which to the authors' knowledge were not fully known in the energy range considered here.

Besides the obvious similarities of protons and antiprotons as projectiles they differ mostly in their capture behavior. First, only antiprotons can annihilate with protons of the atomic nucleus. Since it is known that the process of annihilation is only likely to occur at very low energies [20] it is not included in this investigation. Second, in the case of proton collisions electron capture by the projectile from the target atom is possible. This process plays a dominant role for low-energy collisions. Hence, a two-center approach appears to be most promising for low-energy proton collisions. However, at low energies the present calculations concentrate on antiproton collisions only. Therefore, a basis expansion which is centered solely on the target alkali metal atom for both antiproton and proton projectiles is used. Thereby, limitations pertinent to a molecular approach at high energies are avoided. Furthermore, the same method can be used for antiproton and proton collisions which may be confirmed by a detailed comparison of present proton results with literature data. A detailed analysis of the electron capture process for proton scattering, however, lies beyond

the scope of this work.

The paper is organized as follows: Sec. II explains how the alkali metal atoms are described and reports on the computational approach. Sec. III considers the convergence behavior of the present antiproton and proton results. Subsequently, the calculated cross sections are presented and compared to literature data. Finally, the present results for antiproton–alkali metal collisions are discussed and a comparison with a hydrogen atom as target is made. Sec. IV concludes on the present findings. Atomic units are used unless it is otherwise stated.

II. METHOD

In this work the target atoms are treated as effective one-electron atoms. The valence electron is exposed to a model potential V_{mod} suitable for alkali metal atoms which describes its interaction with the nucleus as well as with the remaining core electrons. Additionally, core polarization effects are included. The employed model potential was proposed by Klapisch [21]. The used potential parameters are given in [22]. The effect of the spin-orbit coupling is not included in the present approach. The energies of the states with principal quantum number $n < 6$ for the alkali metal atoms Li, Na and K which were achieved with this approach are given in table I together with compiled values of the NIST data bank [23]. In the case of energy level splitting due to spin-orbit coupling the present energies are compared to the lower lying reference energies. The largest relative energy splittings of the reference data due to the spin-orbit coupling of the energies given in table I are 0.002 %, 0.1 % and 0.4 % for the energetically lowest lying p states of Li, Na and K, respectively. Particularly for Li there is a very good agreement with the data given by NIST. But also for the other two atoms the deviation from the literature values remains at maximum around one per cent.

In order to describe the collision process the relative motion of the heavy particles is approximated by a classically trajectory (CTA) also referred to as the impact-parameter representation. The projectile is assumed to move on a classical rectilinear trajectory with a constant velocity \mathbf{v} parallel to the z axis. The internuclear distance vector \mathbf{R} is given by $\mathbf{R} = \mathbf{b} + \mathbf{v}t$, where \mathbf{b} is the impact-parameter vector along the x axis and t the time.

The time-dependent Schrödinger equation

$$i \frac{\partial}{\partial t} \Psi(\mathbf{r}, t) = \left(\hat{H}_0 + \hat{V}_{\text{int}}(\mathbf{r}, \mathbf{R}(t)) \right) \Psi(\mathbf{r}, t) \quad (1)$$

of the target atom interacting with the projectile is solved. The atomic Hamiltonian of the target atom is defined as

$$\hat{H}_0 = -\frac{1}{2} \nabla^2 + \hat{V}_{\text{mod}} \quad (2)$$

and the time-dependent interaction between the projec-

$n l$	Li calc.	Na calc.	K calc.
	Li ref. [23]	Na ref. [23]	K ref. [23]
2s	-0.198477		
	-0.198142		
2p	-0.130482		
	-0.130236		
3s	-0.074362	-0.189163	
	-0.074182	-0.188858	
3p	-0.057364	-0.111760	
	-0.057236	-0.111600	
3d	-0.055605	-0.056071	-0.061596
	-0.055606	-0.055937	-0.061397
4s	-0.038694	-0.071754	-0.160105
	-0.038615	-0.071578	-0.159516
4p	-0.032036	-0.051075	-0.100434
	-0.031975	-0.050951	-0.100352
4d	-0.031274	-0.031531	-0.034954
	-0.031274	-0.031442	-0.034686
4f	-0.031254	-0.031267	-0.031337
	-0.031243	-0.031268	-0.031357
5s	-0.023677	-0.037656	-0.064121
	-0.023637	-0.037584	-0.063713
5p	-0.020408	-0.029265	-0.047187
	-0.020374	-0.029202	-0.046969
5d	-0.020013	-0.020160	-0.022158
	-0.020013	-0.020106	-0.021983
5f	-0.020002	-0.020010	-0.020048
	-0.019969	-0.020011	-0.020062

Table I: Calculated binding energies (Hartree) for Li, Na and K using a Klapisch-model potential. The reference data is taken from the NIST data tables [23]. In the case of energy level splitting due to spin-orbit coupling only the energetically lower lying reference energy is given.

tile with the charge Z_p and the target atom as

$$V_{\text{int}}(\mathbf{r}, \mathbf{R}(t)) = \frac{-Z_p}{|\mathbf{r} - \mathbf{R}(t)|} + \frac{Z_p}{|\mathbf{R}(t)|} \quad (3)$$

where \mathbf{r} is the spacial coordinate of the explicitly treated valence electron.

The total wavefunction $\Psi(\mathbf{r}, t)$ is expanded as

$$\Psi(\mathbf{r}, t) = \sum_{nlm} c_{nlm}(t) \phi_{nlm}(\mathbf{r}) \exp(-i \epsilon_{nl} t) \quad (4)$$

using the expansion coefficients $c_{nlm}(t)$. Here, the ϕ_{nlm} are eigenstates of the Hamiltonian \hat{H}_0 with the energy ϵ_{nl} obtained with the model potential. The n , l , m are the principal one-electron quantum number, angular momentum, and its projection on the z axis, respectively. The ϕ_{nlm} can be further expanded as

$$\phi_{nlm}(\mathbf{r}) = g_{nl}(r) \frac{1}{\sqrt{2(1 + \delta_{m,0})}} [(-1)^m Y_l^m(\Omega) + Y_l^m(\Omega)], \quad (5)$$

where the $Y_l^m(\Omega)$ are the spherical harmonics depending on the angular part Ω of \mathbf{r} . In Eq. (5) the symmetry of the Hamiltonian under reflection at the collision plane given by \mathbf{b} and \mathbf{v} is used in order to reduce the number of states. The radial function $g_{nl}(r)$ is further expanded in terms of $(k-1)$ th order B -spline functions. Converged results were found confining the entire space of the electron to a sphere of radius $r_{\max} = 200$ with fixed boundary conditions. The range $[0, r_{\max}]$ is divided into $N_r - 1$ intervals between the knot points ($r_1 = 0, \dots, r_{N_r} = r_{\max}$).

$$g_{nl}(r) = \sum_j^{k+N_r-2} \alpha_{nl}^j \frac{B_j^k(r)}{r} \quad (6)$$

The expansion coefficients α_{nl}^j are determined by diagonalizing the atomic Hamiltonian \hat{H}_0 .

Substitution of the total wavefunction Ψ in Eq. (1) by its expansion given in Eq. (5) results in a system of coupled equations,

$$i \frac{d}{dt} c_{n'l'm'}(t) = \sum_{nlm} c_{nlm}(t) \langle \phi_{n'l'm'} | \hat{V}_{\text{int}} | \phi_{nlm} \rangle \times \exp[i(\epsilon_{n'l'} - \epsilon_{nl})t]. \quad (7)$$

These coupled equations are solved for N_b fixed values of the impact parameter b with the initial condition $c_{nlm}(t = -\infty, b) = \delta_{nlm, n_i l_i m_i}$ where the index $n_i l_i m_i$ represents the initial state of the atom. The transition probability $P_{nlm}(b)$ into the atomic state (n, l, m) after the collision is given by

$$P_{nlm}(b) = |c_{nlm}(t = +\infty, b)|^2. \quad (8)$$

The cross section σ_{nlm} for the transition into the state (nlm) follows from

$$\sigma_{nlm} = 2\pi \int db b P_{nlm}(b). \quad (9)$$

The total cross sections for ionization

$$\sigma_{\text{ion}} = \sum_{\epsilon_{nlm} > 0} \sigma_{nlm} \quad (10)$$

and for excitation of the target atom

$$\sigma_{\text{ex}} = \sum_{\epsilon_{n_i l_i} < \epsilon_{nlm} < 0} \sigma_{nlm} \quad (11)$$

can readily be calculated where $\epsilon_{n_i l_i}$ is the energy of the initial state of the target atom.

III. RESULTS AND DISCUSSION

In what follows, first the convergence behavior and second the dependence of the ionization and excitation cross sections on the impact parameter b for different impact

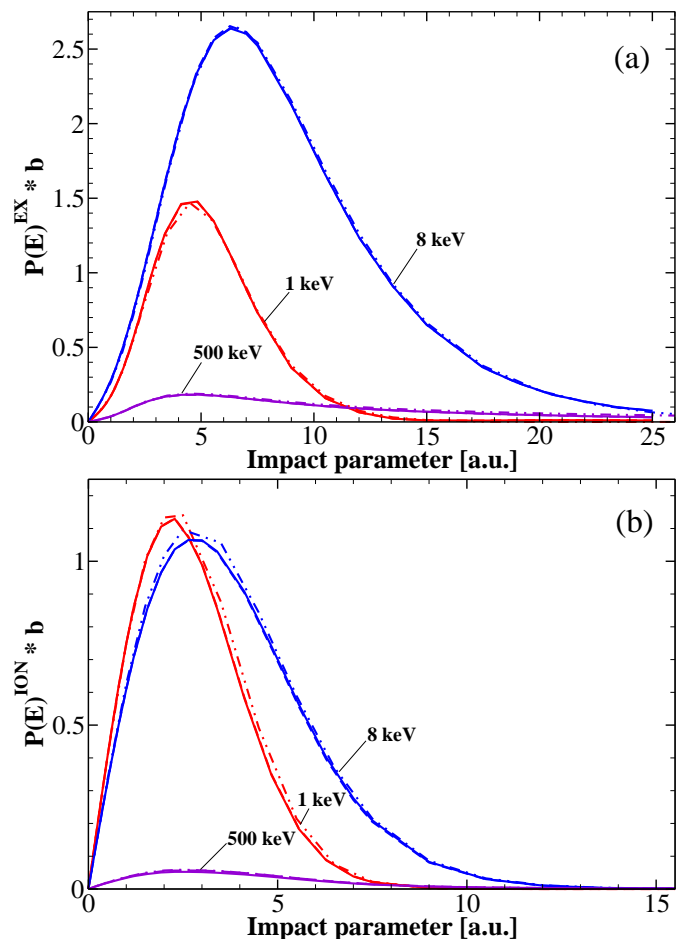


Figure 1: (Color online) \bar{p} - Li(2s) collision: The convergence behavior at different impact energies is shown for the three basis sets A4 (-), A6 (- -) and A8 (· - ·) with maximum angular momenta $l_{\max} = 4, 6$ and 8 , respectively. (a) Total excitation probability $P(E)^{\text{EX}}$ weighted with the impact parameter b as a function of b . (b) As (a), but ionization probability $P(E)^{\text{ION}}$.

energies is investigated. Thereafter, the results for proton and antiproton collisions with the alkali metal target atoms Li, Na and K are presented and the findings are compared with data from literature. Additionally, the antiproton cross sections are compared with calculations including a hydrogen atom as target.

A. Convergence behavior and b -dependent transition probabilities

In order to discuss the convergence of the results the behavior of the product $P(b, E)b$ is investigated. This quantity results after integration over b - cf. Eq. (9) - in the final cross section. Thereby, the probability P for a certain transition depends on the impact parameter b and the impact energy E . In figures 1a and 1b

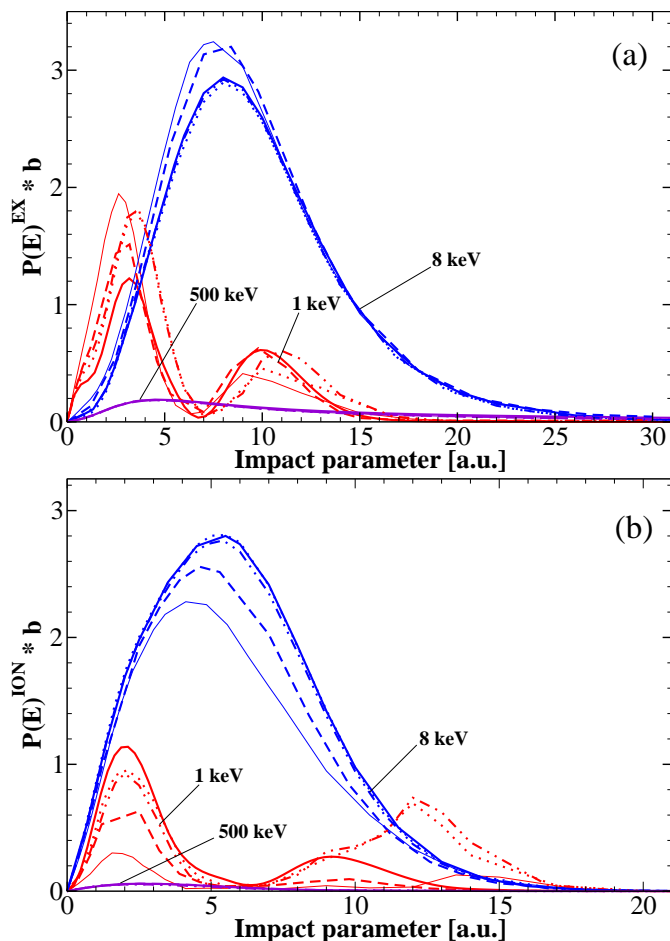


Figure 2: (Color online) p - Li(2s) collision: The convergence behavior at different impact energies is shown for the five different basis sets P6 (-), P8 (- -), P10a (- · - ·), P14 (· · ·) and P10b (-) with maximum angular momenta $l_{\max} = 6, 8, 10, 14$ and 10 , respectively. (a) Total excitation probability $P(E)^{\text{EX}}$ weighted with the impact parameter b as a function of b . (b) As in (a), but ionization probability $P(E)^{\text{ION}}$.

the transition probabilities for total excitation and ionization, respectively, of \bar{p} - Li(2s) collisions calculated for three different energies are presented. The results for p - Li(2s) collisions for the same parameters are shown in figure 2.

In the case of antiproton collisions with lithium calculations for three different basis sets A4, A6 and A8 with maximum angular momenta $l_{\max} = 4, 6$ and 8 , respectively, are shown in figure 1. In table II the maximum angular and magnetic quantum numbers as well as the total number of basis states are given for the basis sets. The calculations using A4 and A6 are fully converged. Therefore, the range of integration has been changed from $-z_{\min} = z_{\max} = 60$ to $-z_{\min} = z_{\max} = 180$ for the calculation using the basis set A8a. This results in slightly higher ionization and lower excitation probabilities at low energies. It was found that the results

for the calculation using $l_{\max} = 8$ converge quickly with increasing maximum projection of the angular momentum m_{\max} . Consequently, for the subsequent calculations dealing with antiprotons as projectile the basis set A8b with $l_{\max} = 8$, $m_{\max} = 3$ and $z_{\max} = 180$ was chosen resulting in a set of 1620 basis functions.

In the case of proton collisions with lithium calculations for five different basis sets P6, P8, P10a, P14 and P10b different basis sets with maximum angular momenta $l_{\max} = 6, 8, 10, 14$ and 10 , respectively, are shown in figure 2. The further parameters of these basis sets are given again in table II. In contrast to the antiproton calculations, much higher angular momenta are needed to achieve convergence – especially for low energies $E \leq 4$ keV. The results for the basis sets P10a and P14 both with $m_{\max} = 3$ seem to be converged with respect to l . Hence, $l_{\max} = 10$ was chosen but m was increased to $m_{\max} = 6$ leading to the basis set P10b. Additionally, the integration range z_{\max} was also enlarged to $z_{\max} = 180$. For all considered energies with $E > 4$ keV these parameters lead to satisfyingly converged results and were therefore used for all proton collision calculations.

From the previous analysis it can be concluded that convergence is achieved much faster (i) for antiprotons than for protons, faster (ii) for excitation than for ionization and (iii) at higher than at lower energies. Figures 1 and 2 also provide insight into the physics of the collision process. For high energies the same behavior for antiproton and proton collisions can be observed. For energies below the validity regime of the first Born approximation the transitions in antiproton collisions take place at smaller impact parameters compared to protons. For close encounters which are more important for low energies the advent of the projectile inside the orbit of the target electrons creates in the case of protons an increased or for antiprotons a decreased binding of the electrons. This situation leads to a decrease (p) or increase (\bar{p}) of P for small b [24] and a shift of the proton P curves to larger b . The ionization probability is for p and \bar{p} more concentrated in the vicinity of the nucleus. This can be explained using the simple picture that the mean velocity of the electrons close to the nucleus is higher than

basis	l_{\max}	m_{\max}	states	basis	l_{\max}	m_{\max}	states
A4	4	4	810	P6	6	6	1188
A6	6	6	1512	P8	8	8	1620
A8a	8	8	2430	P10a	10	3	2052
A8b	8	3	1620	P14	14	3	2916
				P10b	10	6	3024

Table II: Parameters of the basis sets used for the convergence studies. Basis sets beginning with A (P) are used in calculation with antiprotons (protons). For each basis set the maximum angular quantum number l_{\max} , the maximum magnetic quantum number m_{\max} and the total number of basis states are given.

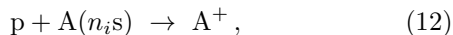
at larger distances and therefore less energy transfer is required. On the other hand the excitation probability has a longer tail for large b compared to ionization. Particularly at high energies care has to be taken that the calculations converge in the considered impact parameter range.

B. Cross sections for proton collisions

Especially for Li atoms but also for Na a number of theoretical and experimental results as well as derived fits exist in literature. Thereby these two collision systems become good candidates to test the used method. Additionally, the results of different theoretical approaches and by that their applicability can be compared. The achieved understanding of the proton systems may be used for the discussion of the antiproton collisions later on for which a thorough comparison is not possible due to the sparseness of literature dealing with antiproton alkali-metal atom collisions. The present results for proton collisions with K complement the sparse literature data for this collision system.

1. Ionization

In figures 3, 4 and 5 the results of the calculations for proton collisions with Li(2s), Na(3s) and K(4s), respectively, are presented. The cross sections for the ionization of alkali metal atoms A,



where A stands for either Li, Na or K initially in their ground states $n_i s$, e.g., Li(2s) are shown in the subfigures 3a, 4a and 5a, respectively. The ionization cross section for proton collisions includes two processes. First the ionization of the alkali metal atom due to electron capture by the proton and second the ionization of the electron into the continuum. The sum of both cross sections is sometimes also referred to as electron loss cross section. The electron capture by the projectile is the dominant process for low energies but vanishes fast with increasing energies and becomes negligible for $E > 100$ keV. For intermediate and high energies the ionization into the continuum is the dominant electron loss process. Therefore, in the following discussion the present ionization calculations are also compared with electron capture cross sections from the literature at low energies and with literature results for ionization excluding electron capture by the proton at high energies.

The present proton ionization cross section for Li(2s) in figure 3a matches perfectly with the 2s contributions of the theoretical ionization cross section by McCartney et al. [18] and also with the experimental results by Shah et al. [3]. The ionization cross section by Schweitzer et al. [1] is somewhat smaller at high energies. The con-

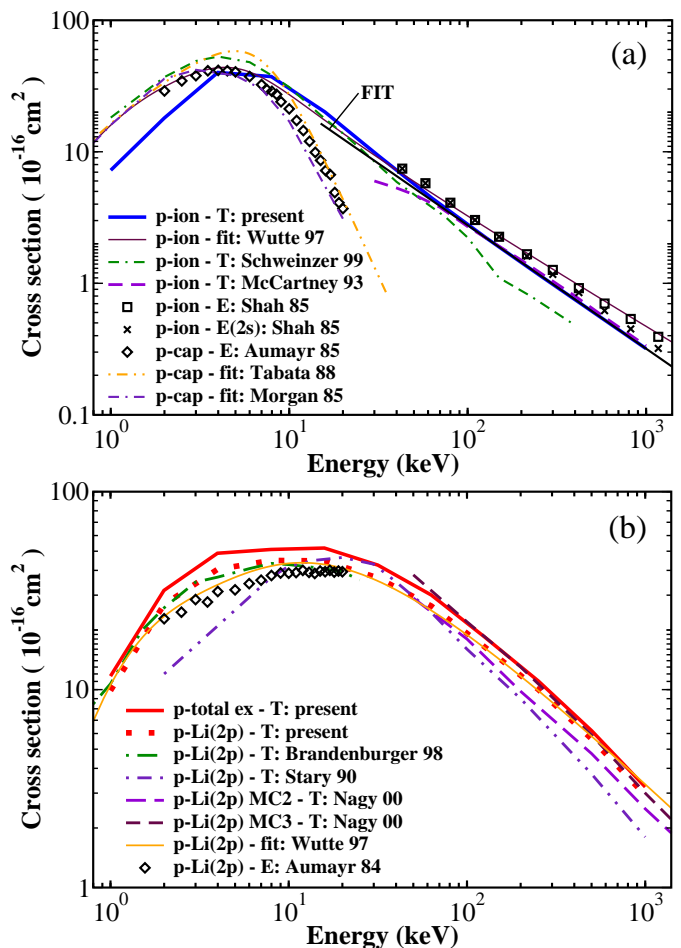


Figure 3: (Color online) p - Li(2s): (a) Ionization and capture. Theory(ionization): solid curve, present results; doubly-dashed dotted curve, Schweitzer et al. [1]; dashed curve, McCartney et al. [18] (Li(2s)). Fit(ionization): thin solid curve, Wutte et al. [2]. Experiment(ionization): squares, Shah et al. [3]; crosses, Shah et al. [3] (Li(2s)). Fit(capture): dashed doubly-dotted curve, Tabata et al. [4]; dashed dotted curve, Morgan et al. [5]. Experiment(capture): diamonds, Aumayr et al. [6]. (b) Total excitation and excitation into Li(2p). Theory(total excitation): solid curve, present results. Theory(excitation into Li(2p)): dotted curve, present results; dashed dotted curve, Brandenburger et al. [7]; dashed doubly-dotted curve, Stary et al. [17]; long-dashed curve, MC2 Nagy et al. [8]; short-dashed curve, MC3 Nagy et al. [8]. Fit(Li(2p)): thin solid curve, Wutte et al. [2]. Experiment(Li(2p)): diamonds, Aumayr et al. [9].

tribution of the 1s electrons to the ionization cross section which is not included in the present calculations has been determined theoretically by Sahoo et al. [25] and McCartney et al. [18] and experimentally by Shah et al. [3]. For energies smaller than 100 keV the contribution of the inner shell becomes negligible compared to the one of the outer shell. For high energies the 1s contribution is in accordance with the difference between the present 2s results and the Li electron ionization cross

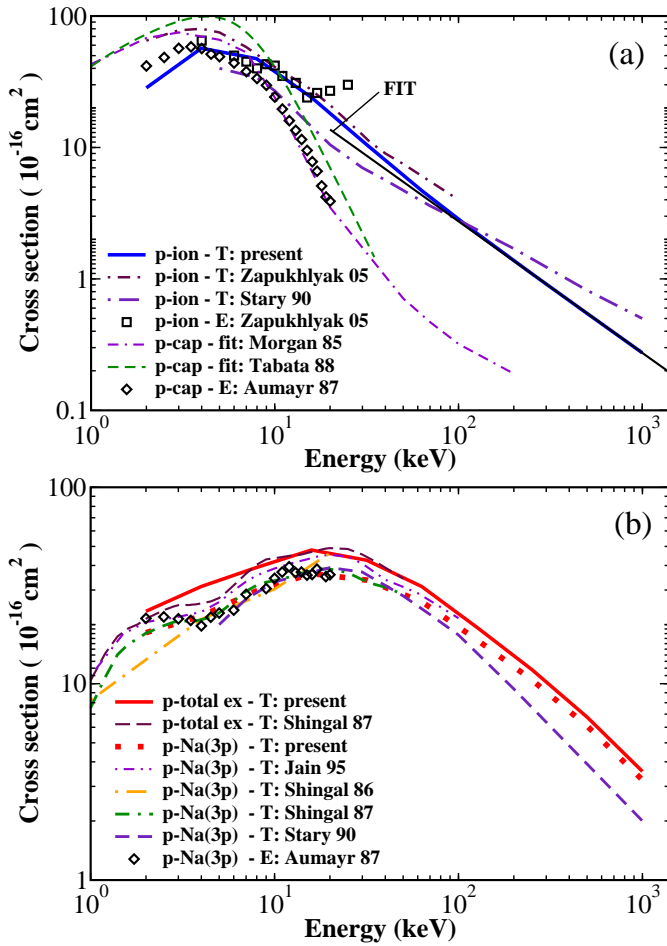


Figure 4: (Color online) p - Na(3s): (a) Ionization and capture. Theory(ionization): solid curve, present results; long-dashed dotted curve, Stary et al. [17]; short-dashed dotted curve, Zapukhlyak et al. [10]. Experiment(ionization): squares, Zapukhlyak et al. [10]. Fit(capture): dashed curve, Tabata et al. [4]; doubly-dashed dotted curve, Morgan et al. [5]. Experiment(capture): diamonds, Aumayr et al. [11]. (b) Total excitation and excitation into Na(3p). Theory(total excitation): solid curve, present results; long-dashed curve, Shingal et al. [12]. Theory(excitation into Na(3p)): dotted curve, present results; dashed doubly-dotted curve, Jain et al. [13]; dashed dotted curve, Shingal et al. [14]; doubly-dashed dotted curve, Shingal et al. [12]; short-dashed curve, Stary et al. [17]. Experiment(Na(3p)): diamonds, Aumayr et al. [11].

section. For energies smaller than 10 keV the electron capture by the proton becomes the dominant ionization process. Down to 4 keV the present findings are in good agreement with literature results shown in figure 3a for capture and ionization. However, for energies smaller than 4 keV the present ionization cross section is clearly smaller than all other shown results. This is in accordance with the difficulty to achieve convergence in the energy range $E \leq 4$ keV for proton collision already discussed in section III A. This may be a consequence of the one-center approach which is expected to converge

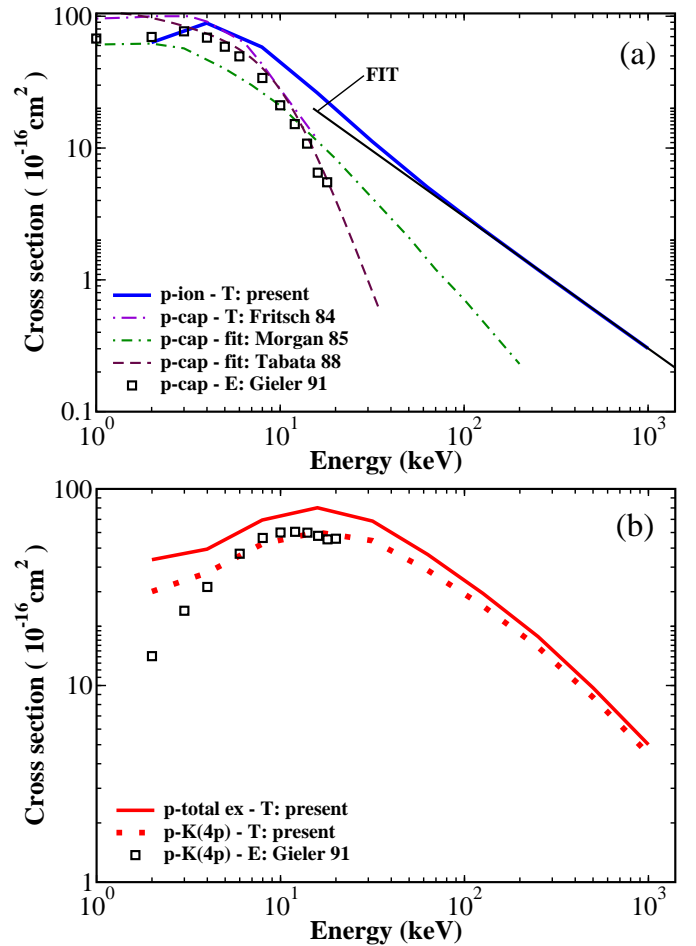


Figure 5: (Color online) p - K(4s): (a) Ionization and capture. Theory(ionization): solid curve, present results. Theory(capture): long-dashed dotted curve, Fritsch [15]. Fit(capture): dashed curve, Tabata et al. [4]; dashed dotted curve, Morgan et al. [5]. Experiment(capture): squares, Gieler et al. [16]. (b) Total excitation and excitation into K(4p). Theory(total excitation): solid curve, present results. Theory(excitation into K(4p)): dotted curve, present results. Experiment(K(4p)): squares, Gieler et al. [16].

slowly when trying to describe the electron capture process properly.

In figure 4a the results for the ionization of the Na atom initially in the ground state are shown. The findings are in good agreement with the recent results by Zapukhlyak et al. [10]. Here, especially their experimentally values match with the present curve except for the three last data points with $E \geq 17$ keV which show an unexpected behavior. Their theoretical ionization cross section agrees for energies higher than 6 keV with the present one but is larger for smaller energies. The cross section of Stary et al. [17] which also covers the range from low to high energies differs from the present findings as well as from the literature results shown here. The data for electron capture by the proton shown here

are consistent with the present findings for the ionization cross section. However, the maximum of the fit by Tabata et al. [4] has a clearly higher value. Again, it can be observed that the present ionization cross section for proton collisions is not fully converged for $E \leq 4$ keV leading to smaller values in this energy range.

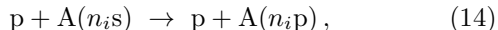
In figure 5a the results of the proton - K(4s) collision calculations are presented. For potassium targets the literature data on proton cross sections are sparse. To the best of the authors' knowledge no ionization cross sections for proton collisions exists. Therefore, the present ionization cross section may be compared with results for electron capture. However, this is only meaningful for low energies $E < 10$ keV where electron capture is the dominant ionization process. The calculations by Fritsch [15], the experimental data measured by Gieler et al. [16] as well as the fit provided by Tabata et al. [4] of the electron capture cross section are in accordance with the present ionization cross section for $E > 4$ keV. The fitted capture cross section by Morgan et al. [5] results in lower values in the relevant energy range between 4 and 10 keV. In the high-energy regime the present cross section shows the same qualitative behavior which already has been observed for Li and Na.

2. Excitation

In the subfigures 3b, 4b and 5b the proton excitation cross sections for Li(2s), Na(3s) and K(4s) are shown. The total excitation of an alkali metal atom A initially in its ground state $n_i s$,



which is the sum of all cross sections for transitions into excited states nl , cf. Eq. (11), is given. Additionally, the cross section for the excitation process into the first excited state $n_i p$ of A,



is given, too. The excitation into the first excited state $n_i p$ is the dominant excitation process especially at high energies. Therefore, there are experimental data for this excitation transition. It was found in the present investigation that it is essential in particular for high energies to extend the range of the impact parameter b to values up to 90 a.u. in order to achieve excitation cross sections which are converged with respect to b . The curves in figures 1 and 2 for 500 keV already indicate that the transition probabilities for excitation vanish slowly with increasing b .

The present proton excitation cross sections for Li(2s) are shown in figure 3b. To the best of the authors' knowledge for p - Li collisions there are no data to compare the present total excitation cross section with. For the excitation into Li(2p) the present results are in good agreement with literature data also shown in figure 3b, except with

the calculations by Stary et al. [17]. Their findings differ for $E < 6$ keV and $E > 100$ keV from all results shown here. The experimental data by Aumayr [9] lie for all energies below the present calculations. On the other hand, the calculations by Brandenburger et al. [7] and also the fit provided by Wutte et al. [2] match with the present data in the whole energy range. Wutte et al. based their fit in the high-energy range on scaled-electron-impact excitation cross sections. The calculations by Nagy et al. [8] were performed with multi-configuration wavefunctions with an orbital basis up to $n = 2$ (MC2) and up to $n = 3$ (MC3).

In figure 4b p - Na(3s) collision cross sections for the total excitation and excitation into the 3p state of the sodium atom initially in the ground state are shown. The theoretical data for the total excitation cross section by Shingal et al. [12] agree well with the present results although they show a feature around 4 keV which is not reproduced by the present findings. However, their excitation cross section into the Na(3p) state follows almost completely the present results – even around 4 keV. The older calculation by Shingal et al. [14] agrees reasonable in the energy range 4 – 14 keV but shows a different behavior for higher and lower energies. Although the calculations of Jain et al. [13] lead for all energies to higher values their qualitative behavior is comparable to the present results. The findings of Stary et al. [17] show the same behavior as their results for p - Li collisions in figure 3b, namely, a cross section which is comparable around the maximum but falls off too fast for higher and lower energies. The experimental data provided by Aumayr et al. [11] is in line with the present cross section for excitation into Na(3p). It also shows a feature around 4 keV.

In figure 5 the results of the present p - K(4s) collision calculations are presented. For excitation into the K(4p) state the experimental findings of Gieler et al. [16] are in good agreement with the present calculations around the maximum but then start to differ for $E \leq 4$ keV. Their data points fall off faster while the present result shows a behavior which has been already observed for p - Na collisions in figure 4b. For Na the slope of the curve changes characteristically around $E = 4$ keV. However, there is no comparable feature for p - Li(2s) collisions. Although the excitation results – in contrast to ionization – for Li and Na collision seem to be reasonable also for low energies it is not possible to quantify how reliable the p - K(4s) excitation cross sections for $E \leq 4$ keV are. The splitting of the energy levels due to spin-orbit coupling which is neglected in the present investigation is supposed to be most relevant for the 4p state of K. However, the good agreement of the present results with the experimental data by Gieler et al. for $E > 4$ keV suggests that the effect due to spin-orbit coupling does not play a major role with respect to the level of accuracy which is achieved by the present method.

In conclusion, the comparison of the present proton ionization and excitation cross sections with literature

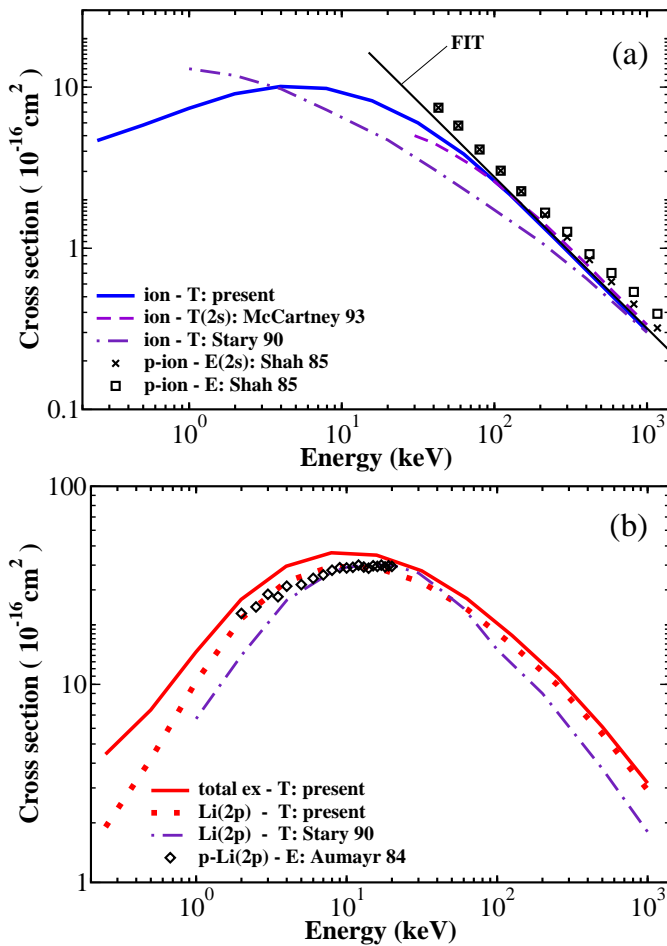


Figure 6: (Color online) \bar{p} - Li(2s): (a) Ionization. Theory: solid curve, present results; dashed dotted curve, Stary et al. [17]; dashed curve, McCartney et al. [18]. Experiment: crosses (p-Li(2s)), Shah et al. [3]; squares (p-Li(2s) and p-Li(1s)), Shah et al. [3]. (b) Total excitation and excitation into Li(2p). Theory(total excitation): solid curve, present results. Theory(excitation into Li(2p)): dotted curve, present results; dashed dotted curve, Stary et al. [17]. Experiment(excitation into Li(2p)): diamonds (p-Li(2s)), Aumayr et al. [9].

data results in a good overall agreement in the energy range $4 \text{ keV} < E < 1000 \text{ keV}$. Thereby, the applicability of the present method is confirmed. The findings by Stary et al. [17], however, differ from the present and the shown literature results. The calculations for p - K collisions complement the data provided by the sparse literature on this collision system.

C. Cross sections for antiproton collisions

Only very few data for antiproton-alkali metal atom collisions exist in the literature. Cross sections are available for the ionization of Li(2s) and Na(3s) as well as for

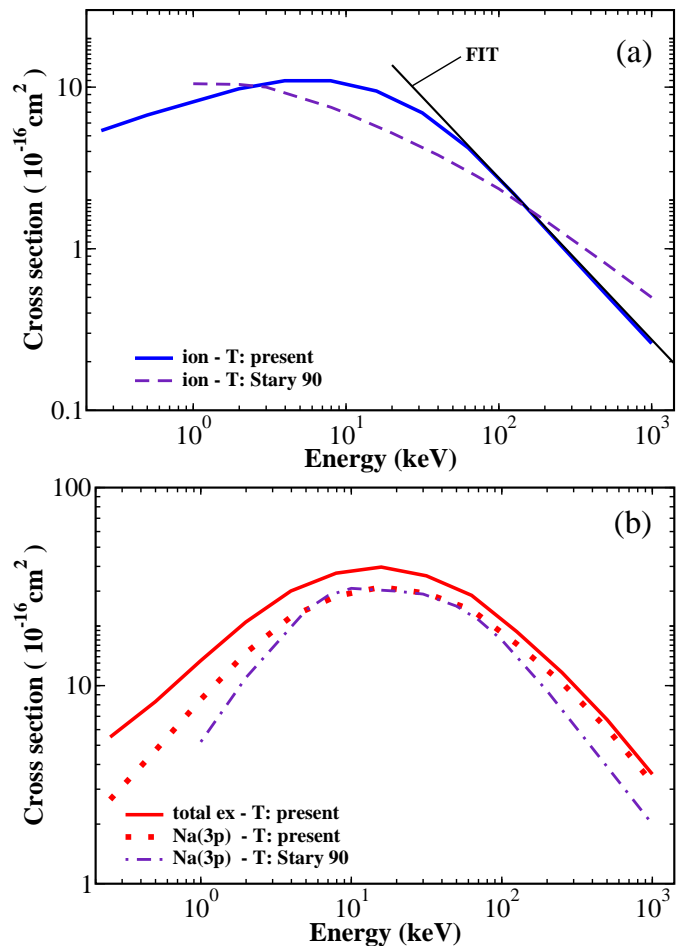


Figure 7: (Color online) \bar{p} - Na(3s) (a) Ionization. Theory: solid curve, present results; dashed curve, Stary et al. [17]. (b) Total excitation and excitation into Na(3p). Theory(total excitation): solid curve, present results. Theory(excitation into Na(3p)): dotted curve, present results.

excitation into Li(2p) and Na(3p) by Stary et al. [17]. Furthermore, there are ionization cross sections for \bar{p} - Li collisions calculated by McCartney et al. [18]. However, no cross section exists for ionization or excitation into K(4p) for K targets and also for all three considered target atoms there are no total excitation cross sections to which the present results could be compared.

1. Ionization and excitation

The ionization cross sections for antiproton collisions with the target atoms Li(2s), Na(3s) and K(4s) are shown in figures 6a, 7a and 8a, respectively, and for excitation accordingly in figures 6b, 7b and 8b. The theoretical results for ionization in \bar{p} - Li collisions by McCartney et al. [18] agree well with the present findings. However, they only cover the high-energy regime $E > 30 \text{ keV}$. The calculated antiproton ionization cross sections for Li and

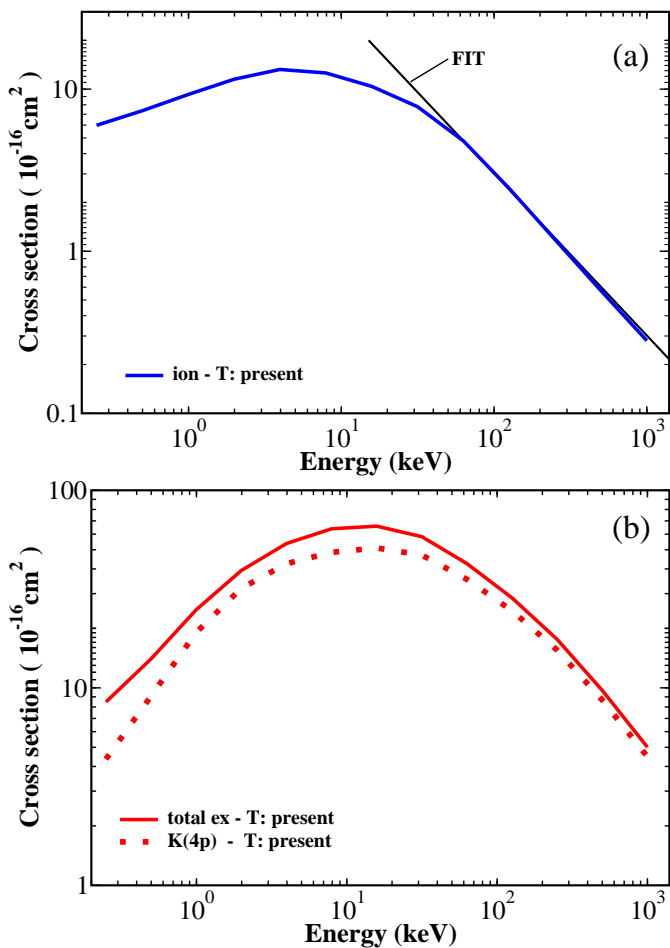


Figure 8: (Color online) \bar{p} - K(4s) (a) Ionization. Theory: solid curve, present results. (b) Total excitation and excitation into K(4p). Theory(total excitation): solid curve, present results. Theory(excitation into K(4p)): dotted curve, present results.

Na targets by Stary et al. [17] both differ considerably from the present findings. Their \bar{p} - Li ionization cross section behaves differently for low to intermediate energies but seems to converge to the present findings for high energies. Their \bar{p} - Na ionization cross section, however, shows a different behavior compared to the present curve in the whole energy range.

The cross sections for the excitation into the first excited state for Li and Na target atoms calculated by Stary et al. [17] both share the same features. Their cross sections agree with the present curves around the maxima at $E \approx 10$ keV and $E \approx 15$ keV for Li and Na, respectively, but fall off faster for lower and higher energies. The same behavior has been observed in the case of proton collisions in figures 3b and 4b for excitations into Li(2p) and Na(3p), respectively. Therefore, their results differ once more from the outcome of the present investigation. The aim of Stary et al. was to obtain results comparable to literature data but using smaller basis sets within

an optical potential approach adapted to this problem. A Feshbach projector formalism for the solution of the time-dependent Schrödinger equation leading to a finite set of coupled-channel equations with complex potentials was used. Thereby, two conditions were assumed to be fulfilled. First, the interactions occur instantaneously and second, the energy distribution of the Q-space which is the complement of the finite model space has a peak leading to the assumption of an average Q-space energy $\bar{\epsilon}$. Furthermore, a scaling factor is used which restores the correct energy dependence of the optical potential and which is determined at high impact energies. Since the present results for the proton case seem to be more reliable than their one-center calculations the present results for antiproton collisions with Li and Na are also considered to be more reliable than theirs. If their solutions are converged as it was claimed by Stary et al. then either not both of the above mentioned conditions are fulfilled or the introduced scaling factor has a different functional behavior.

To the best of the authors' knowledge no literature on \bar{p} - K cross sections exist for the considered energy range. The present cross sections for excitation and ionization of K in figure 8 show a qualitatively similar behavior like for \bar{p} - Na collisions in figure 7 but with higher values throughout the energy range.

Until now, experimental results for the antiproton-alkali metal atom collision systems are completely missing in the considered energy range. It is remarkable that the experimental data of Aumayr [9] for excitation into Li(2p) by proton collisions fits better to the present antiproton than proton data.

2. Comparison of antiproton with proton cross sections

While for sufficiently high energies a similar behavior for proton and antiproton cross sections is to be expected the collision processes should differ for lower energies. In contrary to the proton collisions no electron capture by the projectile is possible for antiprotons. Since the electron capture is the dominant ionization channel for low energy proton collisions noticeable differences especially for the antiproton ionization cross sections can be expected in the low-energy regime. In what follows the antiproton and proton cross sections are compared in some detail for high, intermediate and low impact energies. In figure 9 the ratios of proton to antiproton cross sections for ionization and excitation is given for the three considered target atoms.

To begin with the comparison focuses on the high energy behavior of the antiproton and proton cross sections. In the validity range of the first Born approximation no differences in the cross sections for different projectiles like electrons, protons and antiprotons with the same velocity are expected because in this approximation the cross sections only depend on the absolute value of the projectile charge. It is a high en-

ergy approximation. A linear decrease of the ionization cross section for all three alkali metal atoms can be observed on a doubly-logarithmic scale for high energies $100 \text{ keV} < E < 1000 \text{ keV}$ for protons as well as for antiprotons. Therefore, the general fit formula

$$\sigma_{\text{ion}}(E) = \sigma_{\text{ion}}(E_0) \left(\frac{E}{E_0} \right)^a \quad (15)$$

for ionization cross sections in this energy range can be proposed, where $\sigma_{\text{ion}}(E_0)$ is the ionization cross section for an arbitrary E_0 in the range $100 \text{ keV} < E_0 < 1000 \text{ keV}$ and a is a fit parameter which gives the slope of the linear curve on a doubly-logarithmic scale. The fit parameters which may be proposed for the three alkali metals colliding with protons are given in table III. The fits for Na and K reveal a direct proportionality between the ionization cross section and the inverse of the energy,

$$\sigma_{\text{ion}}(E) = \frac{\sigma_{\text{ion}}(E_0) E_0}{E} \propto \frac{1}{E}, \quad (16)$$

in the considered high energy regime. This proportionality holds approximately also for the present Li ionization cross section. The proposed fits which are also shown in figures 3a, 4a and 5a match well with the calculated ionization cross sections for $E \geq 150 \text{ keV}$. These fits obtained for the proton case are also shown in figures 6a, 7a and 8a in order to compare them with the antiproton ionization cross sections. It can be seen that the proton fits match remarkably well with the antiproton ionization results for energies higher than 150 keV . Therefore, the antiproton ionization cross sections also decrease proportional to E^{-1} where this proportionality again holds only approximately for Li targets. This means that for energies higher than 150 keV no specific features are expected for antiproton ionization cross sections with the considered alkali metal atoms. And in turn for these energies the treatment of proton collisions should be sufficient which is especially in the case of experimental studies less demanding.

However, both systems differ strongly regarding ionization for energies lower than 100 keV due to the electron capture process which is only possible for protons. The proton cross section is strongly enhanced which can also be seen in figure 9. The maxima of the proton and antiproton ionization cross sections approximately at 45

Atom	E_0	$\sigma_{\text{ion}}(E_0)$	a
Li(2s)	141.3	2	-0.9386
Na(3s)	138	2	-1
K(4s)	151	2	-1

Table III: Parameters for the description of the ionization cross section for the energy range $100 \text{ keV} < E_0 < 1000 \text{ keV}$ using the fit formula (15). a is a dimensionless fit parameter. The energy E_0 is given in keV and the cross section $\sigma_{\text{ion}}(E_0)$ for E_0 in units of 10^{-16} cm^2 .

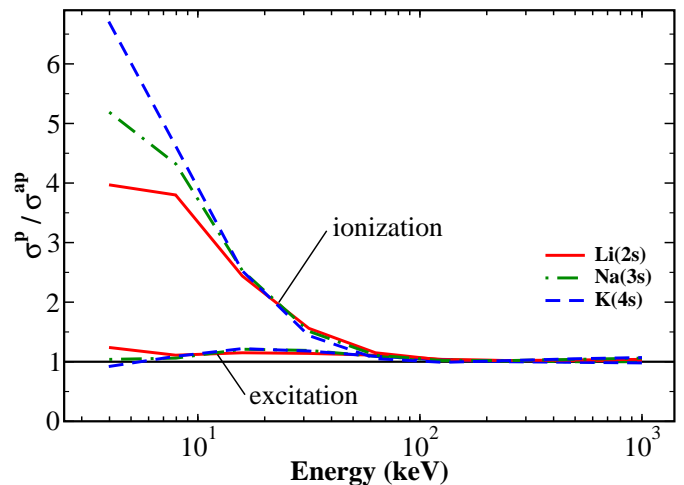


Figure 9: (Color online) Ratio of proton to antiproton cross sections $\sigma^p / \sigma^{\text{ap}}$. The ratios of the ionization and excitation cross sections for the target atoms Li(2s), Na(3s) and K(4s) are given.

and 10 [in 10^{-16} cm^2], respectively, for Li targets differ by a factor 4.5. The ionization maxima for Na and K targets differ approximately by a factor 5.5 and 6.5, respectively. The maxima are all located between 4 and 6 keV where the proton maxima tend to occur at lower energies than the corresponding antiproton maxima.

A comparison of the present excitation cross sections for proton and antiproton collisions yields that they also agree for high energies $E > 150 \text{ keV}$. The antiproton maximum for Li targets lies around 10 keV and is 10% lower than for proton collisions. The antiproton maxima for Na and K are situated at approximately 15 keV with $\approx 20\%$ smaller values than for the proton case. But below their maxima the Na and K excitation curves for antiprotons and protons excitation cross section have comparable values.

The most striking feature of figure 9 is that the ratios of the proton to antiproton ionization cross sections increase strongly for low-energy collisions while the ratios for excitation only vary comparably weakly around 1. In the case of ionization the electron capture channel becomes important for low-energy proton collisions leading to large ionization cross sections compared to antiproton collisions. In the case of excitation for both projectiles the same channels are open.

It can be concluded for the antiproton cross sections that the present results complement and improve the existing data on antiproton-alkali metal atom collisions. While the excitation cross sections are comparable for proton and antiproton projectiles the proton ionization cross sections are strongly enhanced at low energies due to electron capture. For high energies $E > 150 \text{ keV}$ proton and antiproton collisions with Li, Na and K result in the same ionization cross sections which decrease proportional to E^{-1} .

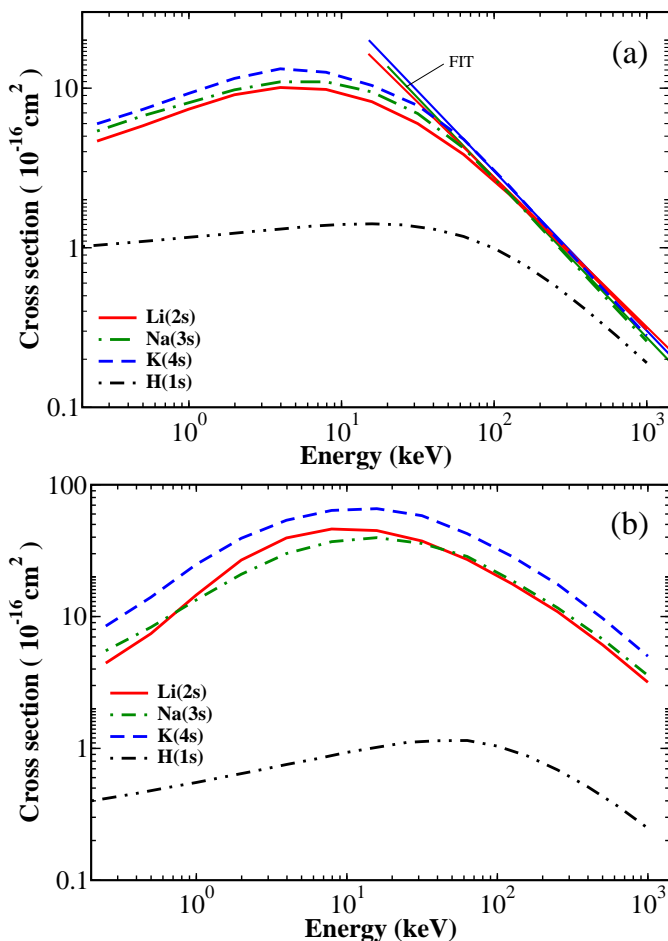


Figure 10: (Color online) (a) Single-electron ionization cross section for antiprotons colliding with Li(2s), solid curve, Na(3s), dashed dotted curve, K(4s), dashed curve, and H(1s), dashed doubly-dotted curve. Additionally, the fits describing the high-energy behavior of proton scattering are given. (b) Total excitation cross section for antiprotons colliding with Li(2s), solid curve, Na(3s), dashed dotted curve, K(4s), dashed curve, and H(1s), dashed doubly-dotted curve.

D. Comparison of the antiproton cross sections

In figure 10a the ionization cross sections for the three alkali metal atoms Li, Na and K colliding with antiprotons are plotted together with the high-energy fits extracted earlier from the proton calculations. The qualitative behavior of the cross sections for these atoms is similar in the whole energy range. All curves converge to their corresponding proton results for energies $E \geq 150$ keV which lie close to each other. The differences between the heights of the ionization cross sections for $E < 100$ keV as well as the ordering of the curves may be explained by the different ionization energies: Li = 0.198, Na = 0.189, K = 0.160 which can also be found in table I. All maxima lie around 4 to 6 keV which is somewhat below the average velocity of the valence electrons and have far lower

values compared to the proton collision systems.

In figure 10b the total excitation cross sections for the three alkali metals are compared. Although the overall behavior of their excitation cross sections are similar they differ in detail. On an absolute scale the values of the antiproton excitation maxima for the three atoms differ considerably [in 10^{-16} cm^2]: Li = 46.2, Na = 39.7, K = 65.9, i.e., the maximum for K is 66% higher than that for Na. This can be made plausible by comparing the energy differences of the ground states to the first excited states: Li = 0.068, Na = 0.089, K = 0.059 since the $n_i s \rightarrow n_i p$ transition is the dominant excitation channel.

The cross sections for ionization and excitation of the hydrogen atom by antiproton impact were also calculated which are presented in figure 10, too. The qualitative behavior of the hydrogen cross sections is comparable to those of the alkali metal atoms reflecting the shell structure of the alkali metal atoms with an outer valence electron in an s state. However, the absolute values of the cross sections differ clearly. First, the cross sections for hydrogen are much smaller due to the tighter binding of the electron which leads to a higher ionization energy and a smaller spacial extension. Second, the maxima are shifted to higher impact energies which can be explained by the higher average velocity of the electron in the ground state of hydrogen. For high energies ($E \geq 1000$ keV) the ionization cross section of hydrogen seem to approach those of the alkali metal atoms. At these energies the ionization cross section of hydrogen is expected to decrease like $E^{-1} \log E$.

IV. CONCLUSION

Time-dependent close-coupling calculations of ionization and excitation cross sections for antiproton and proton collisions with the alkali metal atoms Li(2s), Na(3s) and K(4s) have been performed in a wide energy range from 0.25 to 1000 keV. The target atoms are treated as effective one-electron atoms using a model potential. The total wave function is expanded in an one-center approach in eigenfunctions of the one-electron model Hamiltonian of the target atom. The radial part of the basis functions is expanded in B-spline functions and the angular part in a symmetry-adapted sum of spherical harmonics. The collision process is described in the classical trajectory approximation. In the present calculations the results converged faster for collisions involving antiprotons than protons, faster for high than for low energies and faster for excitation than for ionization. Good agreement with literature data has been achieved for the proton-alkali metal atom cross sections for $E \geq 4$ keV. However, for antiproton-alkali metal atom collisions literature data are sparse. The comparison to the calculations of antiproton collisions with Li and Na by Stary et al. shows the same disagreement with the present findings as it was found for their proton collision results. In view of this disagreement with literature data for proton colli-

sions it can be stated that the calculations by Stary et al. were either not fully converged or the assumed conditions not fulfilled. To the best of the authors' knowledge the first cross sections for \bar{p} - K collisions in the considered energy range are presented. The ionization cross sections for protons and antiprotons differ considerably for energies smaller than 100 keV due to the electron capture process which is only possible for protons and is the dominant ionization channel at low energies. The qualitative behavior of the antiproton cross sections is comparable for all three alkali metal atoms but differs in the absolute values depending on the atom-specific ionization and excitation energies. A comparison with hydrogen as target atom yields the same characteristics as for the alkali metals due to the common s state structure. However,

the cross sections of hydrogen have much lower values and the hydrogen ionization and excitation maxima are shifted to higher impact energies because of the tightly bound 1s electron. For the proton ionization cross sections a simple fit formula is proposed for the energy range from 150 to 1000 keV which also describes the properties of the antiproton ionization cross sections in this energy range well. The fit reveals that the ionization cross sections decrease proportional to E^{-1} in this energy range.

ACKNOWLEDGMENTS

The authors are grateful to BMBF (FLAIR Horizon) and *Stifterverband für die deutsche Wissenschaft* for financial support.

-
- [1] J. Schweinzer, R. Brandenburg, I. Bray, R. Hoekstra, F. Aumayr, R. K. Janev and HP. Winter, *Atomic Data and Nuclear Data Tables* **72**, 239 (1999).
 - [2] D. Wutte, R. K. Janev, F. Aumayr, M. Schneider, J. Schweinzer, J. J. Smith and HP. Winter, *Atomic Data and Nuclear Data Tables* **65**, 155 (1997).
 - [3] M. B. Shah, D. S. Elliott and H. B. Gilbody, *J. Phys. B: At. Mol. Phys.* **18**, 4245 (1985).
 - [4] T. Tabata, R. Ito, N. Yohta, S. Toshizo, S. Masao and S. Toshio, *Nucl. Instr. Meth. Phys. Res. B* **31**, 375 (1988).
 - [5] T. J. Morgan, R. E. Olson, A. S. Schlachter, and J. W. Gallagher, *J. Phys. Chem. Ref. Data* **14**, 971 (1985).
 - [6] F. Aumayr and H. Winter, *Phys. Rev. A* **31**, 67 (1985).
 - [7] R. Brandenburg, J. Schweinzer, F. Aumayr and H. P. Winter, *J. Phys. B: At. Mol. Phys.* **31**, 2585 (1998).
 - [8] L. Nagy and S. Fritzsche, *J. Phys. B: At. Mol. Phys.* **33**, L495 (2000).
 - [9] F. Aumayr, M. Fehring and H. Winter, *J. Phys. B: At. Mol. Phys.* **17**, 4185 (1984).
 - [10] M. Zapukhlyak, T. Kirchner, H. J. Lüdde, S. Knoop, R. Morgenstern and R. Hoekstra, *J. Phys. B: At. Mol. Phys.* **38**, 2353 (2005).
 - [11] F. Aumayr, G. Lakits and H. Winter, *J. Phys. B: At. Mol. Phys.* **20**, 2025 (1987).
 - [12] R. Shingal and B. H. Bransden, *Journal of Physics B: Atomic and Molecular Physics* **20**, 4815 (1987).
 - [13] A. Jain and T. G. Winter, *Phys. Rev. A* **51**, 2963 (1995).
 - [14] R. Shingal, B. H. Bransden, A. M. Ermolaev, D. R. Flower, C. W. Newby and C.J. Noble, *J. Phys. B: At. Mol. Phys.* **19**, 309 (1986).
 - [15] W. Fritsch, *Phys. Rev. A* **30**, 1135 (1984).
 - [16] M. Gieler, P. Ziegelwanger, F. Aumayr, H. Winter and W. Fritsch, *J. Phys. B: At. Mol. Phys.* **24**, 647 (1991).
 - [17] C. Stary, H. J. Lüdde and R. M. Dreizler, *J. Phys. B: At. Mol. Phys.* **23**, 263 (1990).
 - [18] M. McCartney and D. S. F. Crothers, *J. Phys. B: At. Mol. Phys.* **26**, 4561 (1993).
 - [19] FLAIR (Facility for Low-energy Antiproton and Ion Research), <http://www.oeaw.ac.at/smi/flair/> (2007).
 - [20] J. S. Cohen, *Rep. Prog. Phys.* **67**, 1769 (2004).
 - [21] M. Klapisch, *Comput. Phys. Commun.* **2**, 239 (1971).
 - [22] S. Magnier, M. Aubert-Frécon, J. Hanssen, and C. L. Sech, *J. Phys. B: At. Mol. Phys.* **32**, 5639 (1999).
 - [23] NIST (National Institute of Standards and Technology), <http://physics.nist.gov/PhysRefData/ASD/index.html> (2007).
 - [24] H. Knudsen and J. F. Reading, *Phys. Rep.* **212**, 107 (1992).
 - [25] S. Sahoo, R. Das, N. C. Sil, S. C. Mukherjee and K. Roy, *Phys. Rev. A* **62**, 022716 (2000).